Analysis of derivative control based virtual inertia in multi-area high-voltage direct current interconnected power systems

Elyas Rakhshani[1,2] ✉, *Daniel Remon*[1], *Antoni Mir Cantarellas*[1], *Pedro Rodriguez*[1,2]

[1]*Abengoa Research, Abengoa, Campus Palmas Altas, Seville, Spain*
[2]*Electrical Engineering Department, Technical University of Catalonia (UPC), Barcelona, Spain*
✉ *E-mail: elyas.rakhshani@gmail.com*

Abstract: Due to increasing level of power converter-based component and consequently the lack of inertia, automatic generation control (AGC) of interconnected systems is experiencing different challenges. To cope with this challenging issue, a derivative control-based virtual inertia for simulating the dynamic effects of inertia emulations by HVDC (high-voltage direct current) interconnected systems is introduced and reflected in the multi-area AGC system. Derivative control technique is used for higher level applications of inertia emulation. The virtual inertia will add an additional degree of freedom to the system dynamics which makes a considerable improvement on first overshoot responses in addition to damping characteristics of HVDC links. Complete trajectory sensitivities are used to analyse the effects of virtual inertia and derivative control gains on the system stability. The effectiveness of the proposed concept on dynamic improvements is tested through Matlab simulation of two-area test system for different contingencies.

1 Introduction

Automatic generation control (AGC) of a multi-area power system during load and resource variation is known as a very important mechanism that could facilitates frequency restoration and tie-line power flow control between authority areas of AC/DC interconnected systems [1, 2]. The need for transmitting power over long distances with lower losses and higher stability has been always the main challenge for transmission technologies. Due to several limitations associated with AC lines especially for long distance connections and in parallel recent developments of renewable energy integration and super-grid interconnections in modern power systems, attracts a lot of attention to HVDC (high-voltage direct current) transmission, which is known as a proven tool for dealing with the new challenges of future power system [3, 4]. The HVDC interconnection is one of the main applications of power converters in multi-area interconnected power systems which could bring beneficial advantages like: Fast and bidirectional controllability, power oscillation damping (POD) and frequency stability support [5, 6]. For these reasons, in some parts of the world, HVDC or hybrid interconnections, consisting of parallel AC and DC interconnections became already the preferred solution [7, 8] and it is necessary to consider DC links on frequency stability analyses of interconnected power systems.

Usually, conventional generators can provide inertia and governor responses against frequency deviations. Until now several classical and advanced control techniques have been implemented to solve load frequency control (LFC) problem [9–12]. However, in the case of renewable generations, the lack of sufficient inertia will be the main limitation of grid connected renewable electrical energy systems which gives rise to negative impacts on the power system operation [13]. In such complex AC/DC system with the lack of inertia, controlling the power exchange through tie-lines of multi-area interconnected systems makes frequency regulation more complex with several stability problems [14]. It is obvious that the matter of modelling and control considering the methods of providing virtual inertia to the system is critical and the role of advanced technologies such as the use of modern power processing systems, energy storage, and advanced converters in HVDC links will be essential.

Grid-scale energy storage is widely believed to have the potential to provide more flexibility which led to research investigation on both the technical and economic issues surrounding energy storage system (ESS) applications [15–21]. In most of these applications, the matter of inertia and different control methodologies for providing inertia is missing. Recently, several efforts have been carried out to perform virtual inertia with different control methodologies [22–25]. This virtual inertia is emulated by advanced control of power converters considering a short-term energy storage [25] which gave rise to the possibility of having a huge amount of converter-based components without comprising the system stability.

In the generation level, applications of energy storage devices are very important in order to recover the lack of inertia in power electronic parts of generation [26–29] and facilitating renewable sources, especially photovoltaic power plants, to act as a conventional generator for frequency support issues. New concepts like synthetic inertia [30, 31] and virtual synchronous generator are some of the main researches in this part [32]. One application of synthetic inertia emulation for wind power is reported in [31]. In this reference, derivation of frequency is used to modify the references of wind farm generation for providing synthetic inertia emulation. Small-signal analysis and frequency response estimation, both with considering the effects of energy storage and synthetic inertia are also reported by the authors [26, 29], respectively. As reported in [29], estimation of frequency response is considered as complementary task of synthetic inertia to increase the reliability of the system with high wind penetration of power. Most of the works are mainly related to the generation parts of the system and there are no works which focus on transmission and HVDC parts of multi area systems.

In fact, with high penetration of renewables, applications of HVDC interconnections are increased. For two-area AGC power system, AC–DC parallel tie-lines and superconducting magnetic energy storage (SMES) units are proposed in [20, 21]. The HVDC link is used as system interconnection in parallel with AC tie-line to effectively damp the frequency oscillations of AC system while the SMES unit provides bulk energy storage for achieving combined benefits. In these references, there is not any detail about inertia emulation methods and detailed analysis to know the effects and sufficient amount of inertia during contingencies, especially for high level control applications like the AGC of interconnected systems. In [28], a generic modelling is proposed,

but it is not providing enough information about modelling virtual inertia by transmission lines for large area power system. This type of modelling is useful to model each component individually to see the effects on the frequency for isolated system. An Inertia Emulation Control (INEC) system is also proposed in reference [22], which allows voltage source converter (VSC)-HVDC system to perform an inertial response in a similar fashion to synchronous machines.

In this paper, a new application of virtual inertia emulation by converter-based components in multi-area AGC interconnected AC/DC systems is presented. The main objective of this paper is to propose a new approach of frequency stability analysis in multi-area AGC system adding the matter of virtual inertia in AC/DC interconnected systems. In this way, a supplementary power modulation controller (SPMC) is also presented in a coordinated manner for controlling the HVDC set-points during AGC operation. As explained before, traditional LFC models have been modified and revised to add different functionalities in reformulation of conventional power systems. Most of those modifications are related to AGC in a deregulated market scenario [33], different types of power plants like renewable generation [34] and recently the demand side dynamic models [35]. Therefore, the general model of multi-area AGC system will be modified by introducing derivative control technique in AC/DC interconnected AGC model for high level frequency control studies. It should be mentioned that, the importance of the virtual inertia in providing ancillary services like emulating the damping and inertia for frequency control improvements is another motivation of this paper.

Another goal of this paper is to propose a model which is very useful for pre-evaluation of dynamic effects of converter stations in higher level control design for power systems applications. In modern power system, it would be valuable to have a clear idea about the required energy through the transmission line, with proper dynamic analysis considering worst case studies.

2 Dynamic model of multi-area AGC system

2.1 Conventional frequency regulation

In this section, a general overview on modelling and mathematics behind the mechanism of frequency regulation for multi-area interconnected power systems is presented.

2.1.1 Generator-load dynamic model: This model is based on swing equation of synchronous generator where the relation between inertia and load variation will be indicated. The stored energy in the mechanical part of generator is related to rated power (MW) and its inertia constant ($W_{\text{ke}}^0 = H \times S_b$). Considering that kinetic energy is proportional to square of speed (fundamental frequency), the energy for the ($f_0 + \Delta f$) could be calculated as follows

$$W_{\text{ke}} \simeq HS_b\left(1 + \frac{2\Delta f}{f_0}\right)$$
$$\frac{\mathrm{d}}{\mathrm{d}t}(W_{\text{ke}}) = \frac{2HS_b}{f_0}\frac{\mathrm{d}}{\mathrm{d}t}(\Delta f) \tag{1}$$

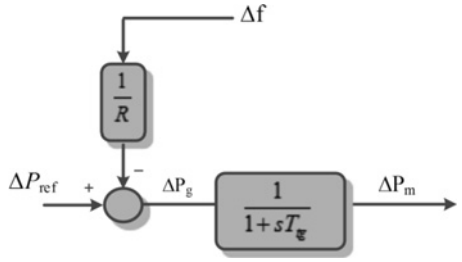

Fig. 1 *Turbine-governor model*

Then the power balance equation could be written as

$$\Delta P_{\text{g}} - \Delta P_{\text{L}} = \frac{2HS_b}{f_0}\frac{\mathrm{d}}{\mathrm{d}t}(\Delta f) \tag{2}$$

and in per unit, Δf is the same as $\Delta\omega$

$$\Delta P_{\text{g}}(\text{pu}) - \Delta P_{\text{L}}(\text{pu}) = 2H\frac{\mathrm{d}}{\mathrm{d}t}\Delta\omega \tag{3}$$

In the dynamic analysis of frequency stability, the most important part of damping is the one related to the sensitivity of load to the frequency variation which is defined as follows

$$\left(\frac{\partial P_{\text{L}}}{\partial f}\right)\Delta f = D \cdot \Delta f$$

where the D (pu/Hz) is the sensitivity of load change for 1% of frequency change and in per unit. Therefore, the complete equation considering the damping in pu will be as follows

$$\Delta P_{\text{g}}(\text{pu}) - \Delta P_{\text{L}}(\text{pu}) = 2H\frac{\mathrm{d}}{\mathrm{d}t}\Delta\omega(\text{pu}) + D(\text{pu}) \cdot \Delta\omega(\text{pu}) \tag{4}$$

Assuming that $T_p = 2H/D$ and $K_p = 1/D$, the equation could be written in the Laplace domain as follows

$$\Delta\omega(s) = \left[\Delta P_{\text{g}}(s) - \Delta P_{\text{L}}(s)\right]\frac{K_P}{1 + sT_P} \tag{5}$$

where T_p is power system time constant and K_p is the gain of power system [2].

2.1.2 Governor-turbine model: As shown in Fig. 1, the output of generator (ΔP_m) in frequency regulation is adjusted by droop governor action and for modelling the governor action a simple first-order function can be used [14]

$$\Delta P_{\text{g}} = \Delta P_{\text{ref}} - \frac{1}{R}\Delta f \tag{6}$$

$$\Delta P_m = \frac{1}{1 + T_{\text{tg}}\,s}\Delta P_{\text{g}} \tag{7}$$

where ΔP_{ref} is coming from area error determining set-points, T_{tg} is the time constant and ΔP_{g} is the input signal for turbine-governor system.

2.1.3 Frequency regulation of interconnected systems: A proper control strategy for active power/frequency issue in large-scale interconnected power systems is shown in Fig. 2. A low-order linearised model is used for modelling the load-generation dynamic behaviours. The angular frequency deviation ($\Delta\omega_i$) for the ith area in pu could be as follows

$$\Delta\omega_i = \frac{K_{pi}}{1 + sT_{pi}}[\Delta P_{mi} - \Delta P_{\text{L}i} - \Delta P_{\text{tie},i}] \tag{8}$$

where ΔP_{mi} is generated power deviation for each generation unit, $\Delta P_{\text{tie},i}$ is the AC tie-line power change and ΔP_{L} is the load change in each area

$$\Delta P_{mi} = \frac{1}{1 + sT_{\text{tg}i}}\left[\frac{-\Delta\omega_i}{R_i} - K_I\, apf_i\, \Delta P_{\text{ref}i}\right] \tag{9}$$

$$\Delta P_{\text{ref}i} = \frac{\text{ACE}_i}{s} \tag{10}$$

and $T_{\text{tg}i}$ is the time constant of turbine-governor of the ith unit, R_i is

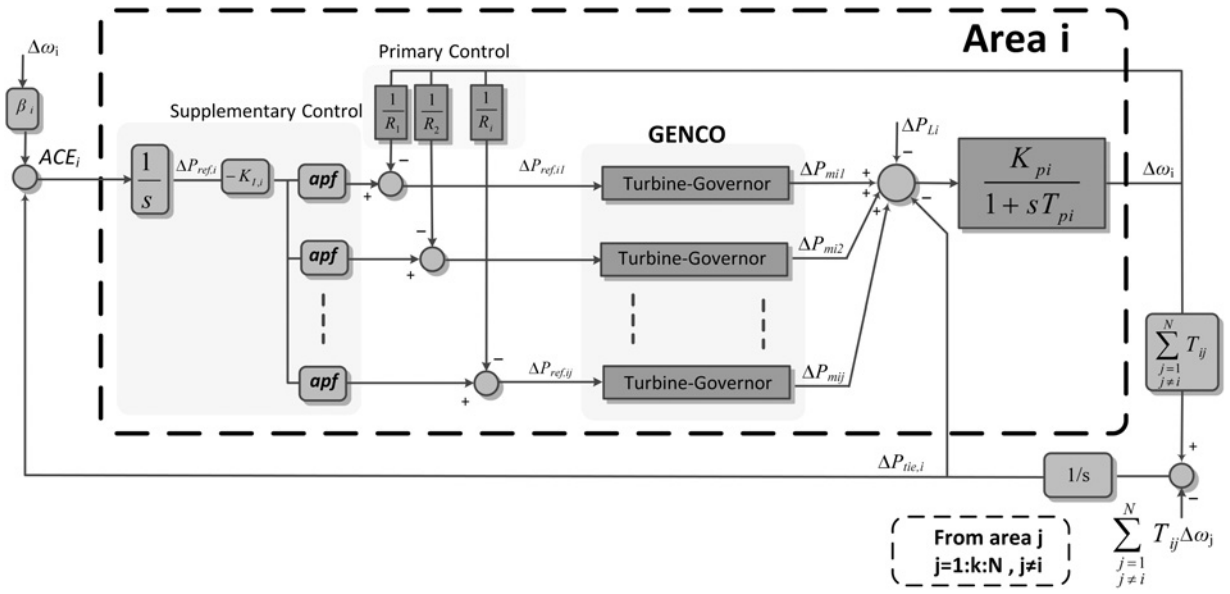

Fig. 2 *Basic frame of ith area in AGC implementation of multi-area AC/DC interconnected power system*

known as droop characteristic, ΔP_{refi} is the reference set-point of units through AGC operation and *ACE* is the area control error expressed as a linear combination of tie-line power flow and weighted frequency deviations adding bias factors (β_i) for each area

$$\text{ACE}_i = \beta_i \Delta\omega_i + \Delta P_{\text{tie},i} \tag{11}$$

In fact, control centres will collect the relevant frequency and power flow information for *ACE* to identify the area participation factors (*apf*) and the appropriate set-point adjustments for each generating unit in AGC.

For modelling the interconnections between N areas in multi-area AGC system, the tie-line power change between area i and the rest of area could be presented as follows [10]

$$\Delta P_{\text{tie},i} = \sum_{\substack{j=1 \\ j\neq i}}^{N} \Delta P_{\text{tieAC},ij} = \frac{1}{s}\left[\sum_{\substack{j=1 \\ j\neq i}}^{N} T_{ij}\Delta\omega_i - \sum_{\substack{j=1 \\ j\neq i}}^{N} T_{ij}\Delta\omega_j\right] \tag{12}$$

$$\Delta P_{\text{tieAC},ji} = \alpha_{ij}\Delta P_{\text{tieAC},ij} \tag{13}$$

$$\alpha_{ij} = -\frac{P_{ri}}{P_{rj}} \tag{14}$$

where T_{ij} is the synchronising coefficient between areas and P_{ri} is the rated power of each area.

2.2 AC/DC transmission model

2.2.1 Brief description of HVDC systems: In two-terminal HVDC transmission, two VSCs are the core of the system. Usually one of the VSCs controls the DC voltage and the other will controls the active power flow. The main control blocks of an averaged VSC, as shown in Fig. 3, are inner and outer control loops. The inner current control of HVDC is a fast dynamic control system for controlling the AC current in this system. The references are provided by outer control.

As shown in Fig. 3, the average model includes of controlled voltage sources on the AC side and controlled current sources on the DC side of converters. A controlled current source is also used for modelling the relationship between AC part and dynamic variations of the DC voltage caused in DC link.

2.2.2 SPMC-based HVDC control in AGC operation: For frequency control analyses, this VSC could be modelled in terms of power transferred from one area to another area through the DC link. Each converter station could be modelled as a first-order transfer function consisting a proper time constant which are related to control blocks presented in Fig. 4. For HVDC system with two VSC stations, the second-order transfer function will be approximated by equivalent first-order transfer function imitating the overall time response of HVDC system as follows

$$\frac{1}{1+s\,T_1}\times\frac{1}{1+s\,T_2} = \frac{1}{1+(T_1+T_2)s+(T_1T_2)s^2} \cong \frac{1}{1+sT_{\text{DC}}} \tag{15}$$

where T_1 and T_2 are the time constants of converters and T_{DC} is the equivalent time constant of overall HVDC control system

$$T_{\text{DC}} = T_1 + T_2 \tag{16}$$

Therefore, the incremental power flow through the HVDC transmission system could be modelled by a linear first-order model with a proper time constant

$$T_{\text{DC}}\frac{\text{d}\Delta P_{\text{DC}}}{\text{d}t} = \Delta x_{\text{r}} - \Delta P_{\text{DC}} \tag{17}$$

where Δx_{r} is the reference control signal of DC power and ΔP_{DC} will be the real DC power flow through the system.

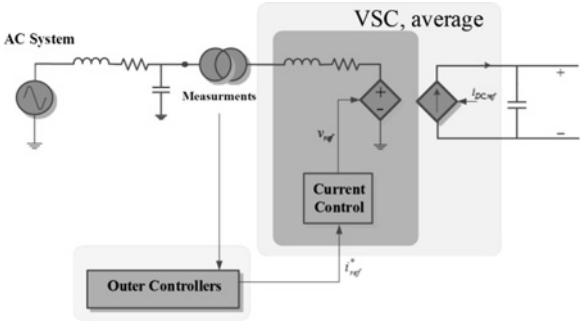

Fig. 3 *Structure of average modelling for each VSC*

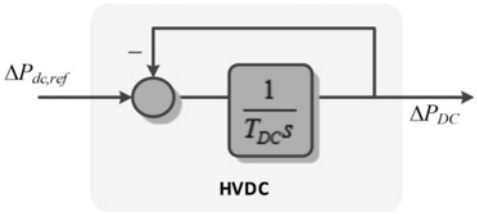

Fig. 4 *Block diagram of the HVDC system*

As mentioned in [12–14], the authors focusing on this type of higher level control design, the proper time response could be between 100 and 500 ms. In this study, the time constant is assumed 300 ms for T_{DC}.

As shown in Fig. 5, in order to implement AGC action, a supplementary modulation controller is designed as higher level damping controller to improve the performance of power system during load changes. The inputs of the proposed SPMC are coming from AGC control centre and the outputs of AGC will generate the new set-points for VSC stations and generation units in all areas.

The Δx_r is the input signal of a HVDC system which will be generated by different control signals. These signals are frequency deviations of each interconnected areas and AC power flow deviations between area i and k ($\Delta P_{tie,ik}$). This power modulation controller is modelled as a proportional controller

$$\Delta x_r = K_{fi}\Delta\omega_i + K_{fk}\Delta\omega_k + K_{AC}\Delta P_{tie,ik} \tag{18}$$

Considering this new state in DC link, the ACE signal of each area in AGC operation which contains one additional HVDC link will be changed as follows

$$\mathrm{ACE}_i = B_i\Delta\omega_i + \Delta P_{tie} \tag{19}$$

$$\Delta P_{tie} = \Delta P_{tie,DC} + \Delta P_{tie,i} \tag{20}$$

where ΔP_{tie} is the total tie-line power deviations, $\Delta P_{tie,i}$ is the tie-line power exchange between area i and other areas and $\Delta P_{tie,DC}$ is the DC power deviation in the HVDC link between area i and area k.

3 Derivative control-based virtual inertia

3.1 Virtual inertia concept

If the derivation signal of the grid frequency is used proportionally for modifying the active power reference of a converter, a virtual inertia in the power system could be emulated which will contribute in enhancing the inertial response of the system against the change in the power demand. The general control law for the active power of the power electronics converter will be as follows

$$P_{\mathrm{emulate}} = k_a\omega_0\frac{\mathrm{d}(\Delta\dot{\omega})}{\mathrm{d}t} \tag{21}$$

where P_{emulate} is the emulated power, k_a is the proportional conversion gain and ω_0 is the nominal grid frequency. This concept could be used for different application like AGC analysis considering a system for providing this virtual inertia to the system [7, 8]. In order to emulate such inertia, an energy source is required. Such energy can be supported from neighbouring area of interconnected system or from an installed ESS. In this study, it is assumed that inertia is emulated through an installed ESS.

3.2 Brief description of energy storage for LFC

As it was explained in the introduction, a variety of battery technologies are being scaled up for grid application [15]. As reported in [17, 18], battery and super-capacitor units can be used for high power applications. Application of SMES as bulk energy storage with HVDC links is also presented in [19, 20]. The application of redox flow type batteries is successfully presented in [36] for two-area interconnected LFC systems. The converter of ESS element will be controlled to keep the storage element charged during normal operation and then help the system during contingencies. In fact, it is assumed that during normal conditions the ESS is fully charged. In the event of a contingency in any area, the ESS automatically will receive an error signal coming from derivation of frequency error. Then it will inject the required power within a very short time. Since the response of ESS is much faster than mechanical part of governors, it is expected that it can affect in a very fast response. It will improve the first overshoot until the rest of conventional reserve in the interconnected areas starts to recover the AGC action. Therefore, the output of ESS will be zero for the steady-state condition.

3.3 Derivative-based virtual inertia for AGC model

To emulate sufficient virtual inertia with power electronic-based component, the control scheme shown in Fig. 6 is proposed. The derivative of the system frequency is obtained and the power reference for converters will be modified. This energy can be provided by storage devices or from reserved capacity of neighbour area. In this study, we assumed that ESS is providing sufficient energy for emulating inertia. This control concept is the derivative control which calculates the rate of change of frequency (ROCOF) during contingencies. The derivative control is sensitive to the noise in the frequency measurements. To solve this problem, a low-pass filter could be added to the control. This filter could also simulate the dynamics of storage device which should be fast. The control law for active power emulation in Laplace with per unit value will be shown in Fig. 6. Where J_i is the control gains of inertia emulation controller and T_{ESS} is also the time constant of added filter for imitating the dynamic control for electronic storage devices. Therefore, the emulated power (ΔP_{ESS})

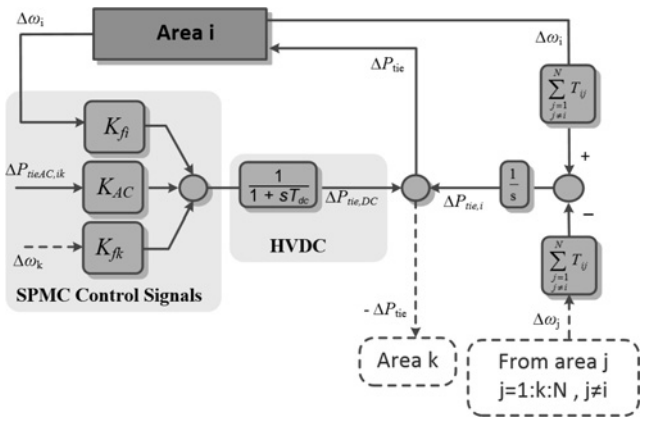

Fig. 5 *Control actions of interconnected area with HVDC model*

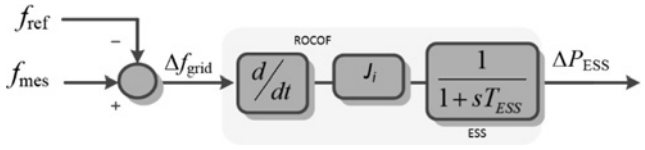

Fig. 6 *Block diagram of derivative inertia emulation*

in term of frequency deviations can be defined like this

$$\Delta P_{\mathrm{ESS1}}(s) = \frac{J_1}{1 + s\,T_{\mathrm{ESS},1}}[s\,\Delta\omega_1(s)] \tag{22}$$

$$\Delta P_{\mathrm{ESS2}}(s) = \frac{J_2}{1 + s\,T_{\mathrm{ESS},2}}[s\,\Delta\omega_2(s)] \tag{23}$$

The control structure for hybrid AC/DC link for interconnected areas with the ability of storing energy and inertia emulation by derivative control is presented in Fig. 7.

As shown in Fig. 7, if the active power through the converter is controlled using the derivative of the frequency, a virtual inertia could be emulated, thus enhancing the inertial response of conventional generator to changes in the power demand. Equations for frequency variations in two-area interconnected AGC system could be modified as follows

$$\Delta\omega_1(s) = \frac{K_{p1}}{1 + sT_{p1}}(\Delta P_{m1} + \Delta P_{m2} - \Delta P_{\mathrm{tieAC},12} - \Delta P_{\mathrm{tie,DC}} + \Delta P_{\mathrm{ESS1}} - \Delta P_{\mathrm{L1}}) \tag{24}$$

$$\Delta\omega_2(s) = \frac{K_{p2}}{1 + sT_{p2}}(\Delta P_{m3} + \Delta P_{m4} + \Delta P_{\mathrm{tieAC},12} + \Delta P_{\mathrm{tie,DC}} + \Delta P_{\mathrm{ESS2}} - \Delta P_{\mathrm{L2}}) \tag{25}$$

It is obvious that with neglecting the damping (D_i) and dynamics of filter in the emulated power signal, these equations for the ith area could be simplified as follows

$$(M_i + J_i)\frac{\mathrm{d}\Delta\omega_i}{\mathrm{d}t} = \Delta P_a \tag{26}$$

where ΔP_a is the total accelerating power. Considering (26) for better understanding of added inertia, it is clear that using derivative control technique, the total inertia ($M_i + J_i$) of the system can be increased.

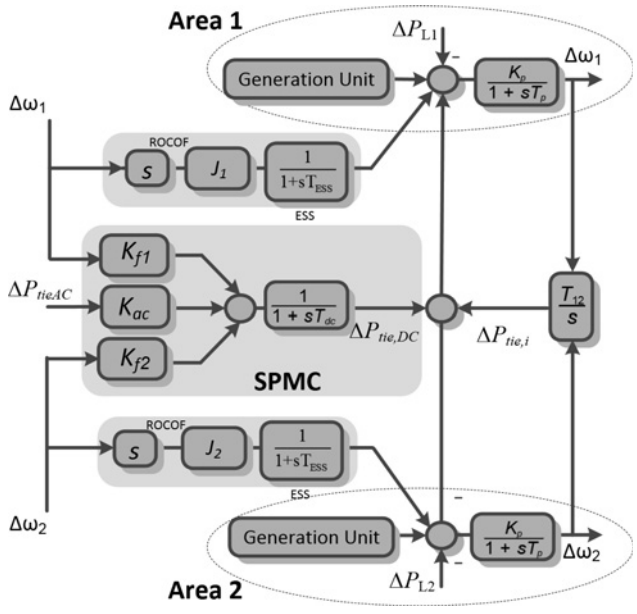

Fig. 7 *Proposed model for two-area AC/DC interconnected system*

The rest of the equation for the two-area system will be as follows

$$\Delta P_{m1}(s) = \frac{1}{1 + sT_{\mathrm{tg1}}}\left[\frac{\Delta\omega_1}{R_2 \times 2\pi} - K_{I1}\Delta P_{\mathrm{ref1}}\right] \tag{27}$$

$$\Delta P_{m2}(s) = \frac{1}{1 + sT_{\mathrm{tg2}}}\left[\frac{\Delta\omega_2}{R_2 \times 2\pi} - K_{I1}\Delta P_{\mathrm{ref1}}\right] \tag{28}$$

$$\Delta P_{m3}(s) = \frac{1}{1 + sT_{\mathrm{tg3}}}\left[\frac{\Delta\omega_3}{R_3 \times 2\pi} - K_{I2}\Delta P_{\mathrm{ref2}}\right] \tag{29}$$

$$\Delta P_{m4}(s) = \frac{1}{1 + sT_{\mathrm{tg4}}}\left[\frac{\Delta\omega_4}{R_4 \times 2\pi} - K_{I2}\Delta P_{\mathrm{ref2}}\right] \tag{30}$$

$$\Delta P_{\mathrm{ref1}} = \frac{\mathrm{ACE}_1}{s} = \frac{1}{s}\left[\frac{\beta_1}{2\pi}\Delta\omega_1 + \Delta P_{\mathrm{tieAC},12} + \Delta P_{\mathrm{tie,DC}}\right] \tag{31}$$

$$\Delta P_{\mathrm{ref2}} = \frac{\mathrm{ACE}_2}{s} = \frac{1}{s}\left[\frac{\beta_2}{2\pi}\Delta\omega_2 - \Delta P_{\mathrm{tieAC},12} - \Delta P_{\mathrm{tie,DC}}\right] \tag{32}$$

$$\Delta P_{\mathrm{tie,AC}} = \frac{T_{12}}{s}\left[\Delta\omega_1 - \Delta\omega_2\right] \tag{33}$$

$$\Delta P_{\mathrm{tie,DC}} = \frac{1}{1 + sT_{\mathrm{DC}}}\left[K_{f1}\Delta\omega_1 + K_{f2}\Delta\omega_2 + K_{\mathrm{AC}}\Delta P_{\mathrm{tieAC},12}\right] \tag{34}$$

To perform detailed analysis for the two-area power system, the complete state-space presentation of the studied system should be performed. The state space form can be obtained considering (22)–(34)

$$\dot{\boldsymbol{x}} = \boldsymbol{A}\boldsymbol{x} + \boldsymbol{B}\boldsymbol{u} \tag{35}$$

where the state matrix $\boldsymbol{A}$ is partitioned as follows

$$\boldsymbol{A} = \begin{bmatrix} \boldsymbol{A}_{11} & \boldsymbol{A}_{12} \\ \boldsymbol{A}_{21} & \boldsymbol{A}_{22} \\ \boldsymbol{A}_{31} & \boldsymbol{A}_{32} \end{bmatrix}_{(12\times12)} \tag{36}$$

Therefore, each sub-matrix will be as follows: (see (equation 37) at the bottom of the next page)

As identified in state-space presentation of global system, the parameters of derivative control (J_1 and J_2) are appeared in sub-matrices $\boldsymbol{A}_{31}$ and $\boldsymbol{A}_{32}$ which are related to derivative control state variables. In fact, these parameters are presented in 11th and 12th rows of the global system matrix $\boldsymbol{A}$ and could be used in analysing the system performance. These elements are as follows

$$a_{11,1} = \frac{-J_1}{T_{\mathrm{ess1}}T_{p1}},\quad a_{11,3} = \frac{J_1 K_{p1}}{T_{\mathrm{ess1}}T_{p1}},\quad a_{11,4} = \frac{J_1 K_{p1}}{T_{\mathrm{ess1}}T_{p1}},$$
$$a_{11,9} = \frac{J_1 K_{p1}}{T_{\mathrm{ess1}}T_{p1}},\quad a_{11,10} = \frac{J_1 K_{p1}}{T_{\mathrm{ess1}}T_{p1}},\quad a_{11,11} = \frac{-J_1 K_{p1}}{T_{\mathrm{ess1}}T_{p1}} + \frac{-1}{T_{\mathrm{ess1}}},$$
$$a_{12,2} = \frac{-J_2}{T_{\mathrm{ess2}}T_{p2}},\quad a_{12,5} = \frac{J_2 K_{p2}}{T_{\mathrm{ess2}}T_{p2}},\quad a_{12,6} = \frac{J_2 K_{p2}}{T_{\mathrm{ess2}}T_{p2}},$$
$$a_{12,9} = \frac{J_2 K_{p2}}{T_{\mathrm{ess2}}T_{p2}},\quad a_{12,10} = \frac{J_2 K_{p2}}{T_{\mathrm{ess2}}T_{p2}},\quad a_{12,12} = \frac{-J_2 K_{p2}}{T_{\mathrm{ess2}}T_{p2}} + \frac{-1}{T_{\mathrm{ess2}}} \tag{38}$$

Finally, the $\boldsymbol{B}$ matrix can be presented as follows where the control

vector consists of load variations in each area

$$\boldsymbol{B} = \begin{bmatrix} \frac{-K_{P1}}{T_{P1}} & 0 \\ 0 & \frac{-K_{P2}}{T_{P2}} \\ 0 & 0 \\ \vdots & \vdots \\ 0 & 0 \\ \frac{-J_1 K_{p1}}{T_{\text{ess1}} T_{p1}} & 0 \\ 0 & \frac{-J_2 K_{p2}}{T_{\text{ess2}} T_{p2}} \end{bmatrix}_{(12\times 2)} \tag{39}$$

As shown in this model, we will have two more gains (J_1 and J_2) related to inertia emulators for both areas. Usually, it would be possible to define a cost function for obtaining the optimum values for these control gains. These gains could be defined based on optimisation theory by minimising the following cost function [10–12]

$$J = \int^{\left[\text{ACE}_1^2 + \text{ACE}_2^2\right]} \mathrm{d}t \tag{40}$$

This cost function is the regular function which is based on the ISE (integral of squared error) method [12, 13]. The control parameter for this case study could be obtained using (40) and classical FMINCON function in Matlab software.

4 System analysis

As shown in Fig. 8, a generic two-area power system which consists of two generation units and one load centre in each area is used for higher level of control applications. As shown in this figure, AGC and (Energy Management Systems) EMS are part of the control centre. The studied model consists of parallel AC and HVDC lines with ESS. In the ESS model, the power electronics are assumed as interface to control storage behaviour in response to AGC signals to improve the frequency oscillations.

The effect of derivative control in two-area system is analysed by performing the numerical analysis, parameter and eigensensitivity (modal) analysis. All the analyses are performed in Matlab platform and the system parameters are given by Rakhshani and Rodriguez [14]. It is assumed that the load contingency is happening in area one by demanding 0.03 pu step load at 5 s. It should be mentioned that the main objective of this section is to analyse the effects of derivative control gains on the performance of the system.

4.1 Sensitivity analysis

4.1.1 Parameter sensitivity: To analyse the effects of control gain on the system behaviour, numerical simulation is performed with different values of control gain J. The effects on the power system frequency characteristics are illustrated in Fig. 9. When the J_1 value is increasing (from 0.1 to 2.9), the peak of frequency is reducing as expected. However, at the same time an important increase in the settling times is observable, especially for the values higher than 0.8 pu.

The effects of control gain over damping and frequency of oscillatory modes are also presented in Table 1. It is obvious that by increasing the control gain, better damping with less oscillation is obtained.

4.1.2 Eigensensitivity: The main objective in eigenvalue sensitivity analysis is to identify the sensitivity of eigenvalues to each element of state matrix $\boldsymbol{A}$ in the system. Calculation of participation matrix will be another part to identify the participants on each sensitive mode. These participations are presented in Table 2.

$$\boldsymbol{A}_{11} = \begin{bmatrix} \frac{-1}{T_{P1}} & 0 & \frac{K_{P1}}{T_{P1}} & \frac{K_{P1}}{T_{P1}} & 0 & 0 & 0 & 0 \\ 0 & \frac{-1}{T_{P2}} & 0 & 0 & \frac{K_{P2}}{T_{P2}} & \frac{K_{P2}}{T_{P2}} & 0 & 0 \\ \frac{-1}{2\pi R_1 T_{\text{tg1}}} & 0 & \frac{-1}{T_{\text{tg1}}} & 0 & 0 & 0 & \frac{-K_{I1}}{T_{\text{tg1}}} & 0 \\ \frac{-1}{2\pi R_2 T_{\text{tg2}}} & 0 & 0 & \frac{-1}{T_{\text{tg2}}} & 0 & 0 & \frac{-K_{I1}}{T_{\text{tg2}}} & 0 \\ 0 & \frac{-1}{2\pi R_3 T_{\text{tg3}}} & 0 & 0 & \frac{-1}{T_{\text{tg3}}} & 0 & 0 & \frac{-K_{I2}}{T_{\text{tg3}}} \\ 0 & \frac{-1}{2\pi R_4 T_{\text{tg4}}} & 0 & 0 & 0 & \frac{-1}{T_{\text{tg4}}} & 0 & \frac{-K_{I2}}{T_{\text{tg4}}} \end{bmatrix}_{(6\times 8)}$$

$$\boldsymbol{A}_{12} = \begin{bmatrix} \frac{-K_{P1}}{T_{P1}} & \frac{-K_{P1}}{T_{P1}} & \frac{-K_{P1}}{T_{P1}} & 0 \\ \frac{-K_{P2}}{T_{P2}} & \frac{-K_{P2}}{T_{P2}} & 0 & \frac{-K_{P2}}{T_{P2}} \\ 0 & 0 & 0 & 0 \\ \vdots & \vdots & \vdots & \vdots \\ 0 & 0 & 0 & 0 \end{bmatrix}_{(6\times 4)}, \quad \boldsymbol{A}_{21} = \begin{bmatrix} \frac{\beta_1}{2\pi} & 0 & 0 & \dots & 0 \\ 0 & \frac{\beta_2}{2\pi} & 0 & \dots & 0 \\ \frac{T_{12}}{2\pi} & \frac{-T_{12}}{2\pi} & 0 & \dots & 0 \\ \frac{K_{f1}}{T_{\text{DC}}} & \frac{K_{f2}}{T_{\text{DC}}} & 0 & \dots & 0 \end{bmatrix}_{(4\times 8)}, \tag{37}$$

$$\boldsymbol{A}_{22} = \begin{bmatrix} 1 & 1 & 0 & 0 \\ -1 & -1 & 0 & 0 \\ 0 & 0 & 0 & 0 \\ \frac{K_{\text{AC}}}{T_{\text{DC}}} & \frac{-1}{T_{\text{DC}}} & 0 & 0 \end{bmatrix}_{(4\times 4)}, \quad \boldsymbol{A}_{32} = \begin{bmatrix} \alpha_{11.9} & \alpha_{11.10} & \alpha_{11.11} & 0 \\ \alpha_{12.9} & \alpha_{12.10} & 0 & \alpha_{11.12} \end{bmatrix}_{(2\times 4)}$$

$$\boldsymbol{A}_{31} = \begin{bmatrix} \alpha_{11.1} & 0 & \alpha_{11.3} & \alpha_{11.4} & 0 & 0 & 0 & 0 \\ 0 & \alpha_{12.2} & 0 & 0 & \alpha_{12.5} & \alpha_{12.6} & 0 & 0 \end{bmatrix}_{(2\times 8)}$$

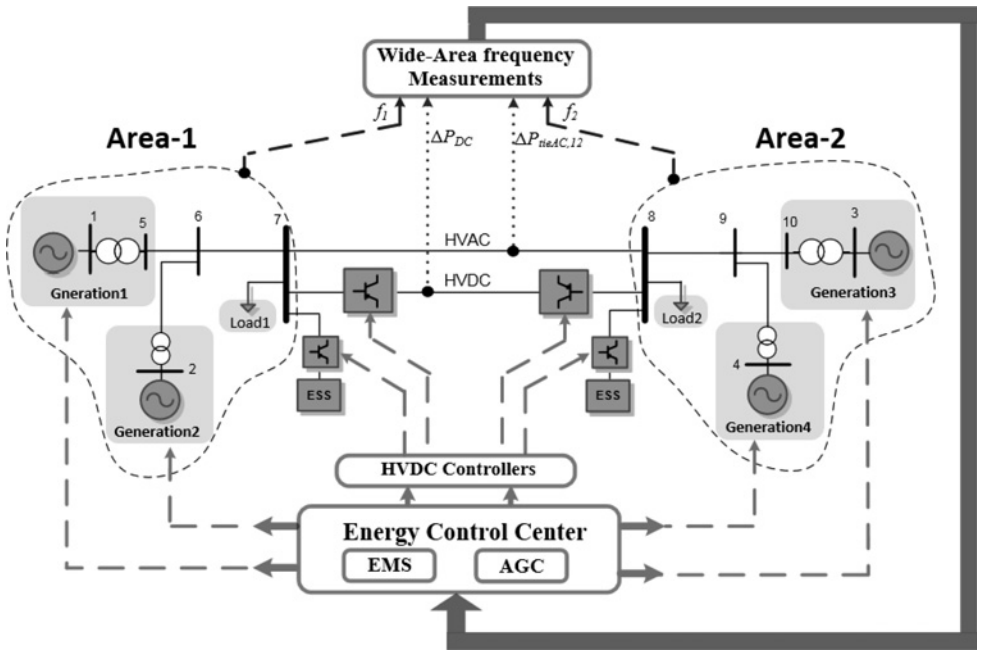

Fig. 8 *Configuration of the power system with high level control and HVDC link*

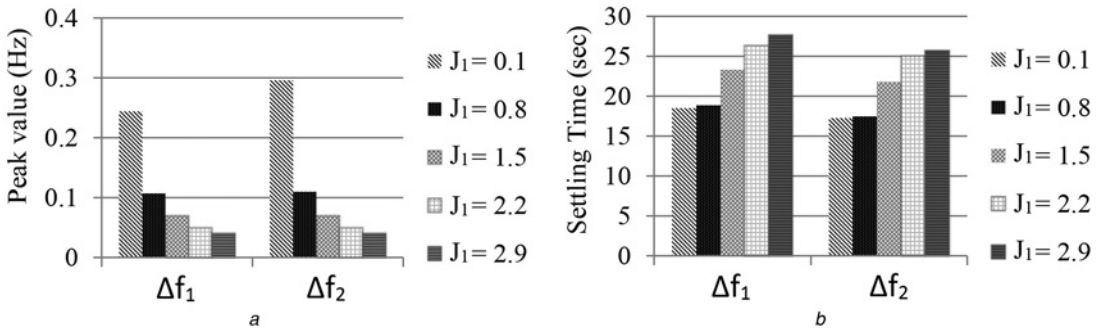

Fig. 9 *Frequency response characteristics in two-area system*

a Peak overshoot
b Settling time

Based on the obtained result, it can be observed that exactly which states have more participation in sensitive or critical modes. For example one of the oscillatory modes from the eigenvalue analysis is $\lambda_{4,5}$ and by checking the participation factor matrix it is clear that $\Delta\omega_1$ and $\Delta\omega_2$ have the most participation in those modes.

Therefore, the best way to change the *i*th mode is to apply a control on the state variable such that the above sensitivity has the largest participating factor.

As explained, the parameters of derivative control are appeared in sub-matrices $\boldsymbol{A}_{31}$ and $\boldsymbol{A}_{32}$, in 11th and 12th rows of the state matrix $\boldsymbol{A}$. The results of sensitivities to these parameters are presented in Tables 3 and 4.

The main objective of Tables 3 and 4 is to present the highest sensitivity of each element regarding the eigenvalues of the overall system. For example, as it can be observed in Table 4, the $\boldsymbol{\alpha}_{12,12}$ parameter has the main sensitivity for second eigenvalue of the system.

Table 1 Control parameters for studied model

Index		$J_1 = 0.8$	$J_1 = 1.5$	$J_1 = 2.2$	$J_1 = 2.9$
damping of oscillatory modes	$\zeta_{\lambda_{4,5}}$	0.5252	0.5446	0.5524	0.5566
	$\zeta_{\lambda_{7,8}}$	0.6273	0.6933	0.7114	0.7190
frequency of oscillatory modes	$f_{\lambda_{4,5}}$	0.3024	0.3017	0.3013	0.3010
	$f_{\lambda_{7,8}}$	0.0377	0.0354	0.0350	0.0349

The summary of the eigenvalue sensitivity analysis is presented in Table 5. As shown by sensitivity matrices, $\boldsymbol{\lambda}_1$ and $\boldsymbol{\lambda}_2$ have the main sensitivity. Considering the results of participation matrix, it is indicated that controlling the 11th and 12th states are the most important ones for control design.

As explained before, these two states (ΔP_{ess1} and ΔP_{ess2}) are affected by their control gains J_1 and J_2, respectively. So with proper selection of these two gains, the desired dynamic response could be obtained. For exploring the proper range of control gain parameters, three-dimensional (3D) presentations of system

Table 2 Sensitivity of each mode for important elements of $\boldsymbol{A}$ matrix

Modes	Associated states	Participation factors
$\boldsymbol{\lambda}_1$	$\Delta \boldsymbol{P}_{ESS1}$	**0.9982**
$\boldsymbol{\lambda}_2$	$\Delta \boldsymbol{P}_{ESS2}$	**1.0054**
$\boldsymbol{\lambda}_3$	$\Delta P_{tie,DC}$, $\Delta\omega_1$, $\Delta\omega_2$	1.1053, 0.1517, 0.036
$\boldsymbol{\lambda}_4$	$\Delta P_{tie,AC}$, $\Delta\omega_1$, $\Delta\omega_2$	0.3661, 0.8140, 0.402
$\boldsymbol{\lambda}_5$	$\Delta P_{tie,AC}$, $\Delta\omega_1$, $\Delta\omega_2$	0.3661, 0.8140, 0.402
$\boldsymbol{\lambda}_6$	$\Delta \boldsymbol{ACE}_1$, $\Delta\omega_1$, $\Delta\omega_2$	**1.2578, 0.3975, 0.220**
$\boldsymbol{\lambda}_7$	ΔACE_2, $\Delta\omega_1$, $\Delta\omega_2$	0.5801, 0.4537, 0.544
$\boldsymbol{\lambda}_8$	ΔACE_2, $\Delta\omega_1$, $\Delta\omega_2$	0.5801, 0.4537, 0.544
$\boldsymbol{\lambda}_9$	ΔP_{m3}, ΔP_{m4}	0.8498, 0.3692
$\boldsymbol{\lambda}_{10}$	ΔP_{m1}, ΔP_{m2}	0.5184, 0.4850
$\boldsymbol{\lambda}_{11}$	ΔP_{m3}, ΔP_{m4}	0.7504, 0.2589
$\boldsymbol{\lambda}_{12}$	ΔP_{m1}, ΔP_{m2}	0.4830, 0.5170

Table 3 Sensitivity of each mode for important elements of ***A*** matrix

Absolute sensitivity	$\alpha_{11,1}$	$\alpha_{11,3}$	$\alpha_{11,4}$	$\alpha_{11,9}$	$\alpha_{11,10}$	$\alpha_{11,11}$
λ_1	0.0243	0.000	0.000	0.000	0.000	**0.9982**
λ_2	0.000	0.000	0.000	0.000	0.000	0.000
λ_3	0.0041	0.000	0.000	0.000	0.096	0.0088
λ_4	0.020	0.000	0.000	0.000	0.0044	0.0029
λ_5	0.020	0.000	0.000	0.000	0.0044	0.0029
λ_6	0.0097	0.0021	0.0021	0.000	0.0011	0.0038
λ_7	0.0111	0.000	0.000	0.000	0.000	0.0014
λ_8	0.0111	0.000	0.000	0.000	0.000	0.0014
λ_9	0.0016	0.000	0.000	0.000	0.000	0.000
λ_{10}	0.0022	0.0019	0.0017	0.000	0.000	0.0028
λ_{11}	0.000	0.000	0.000	0.000	0.000	0.000
λ_{12}	0.000	0.000	0.000	0.000	0.000	0.000

Table 4 Sensitivity of each mode for important elements of ***A*** matrix

Absolute sensitivity	$\alpha_{12,2}$	$\alpha_{12,5}$	$\alpha_{12,6}$	$\alpha_{12,9}$	$\alpha_{12,10}$	$\alpha_{12,12}$
λ_1	0.000	0.000	0.000	0.000	0.000	0.000
λ_2	0.0780	0.000	0.000	0.000	0.0069	**1.0051**
λ_3	0.0049	0.000	0.000	0.000	0.0183	0.0087
λ_4	0.0317	0.000	0.000	0.0022	0.0131	0.0041
λ_5	0.0317	0.000	0.000	0.0022	0.0131	0.0041
λ_6	0.0170	0.0015	0.0015	0.0012	0.0024	0.0012
λ_7	0.0421	0.0033	0.0031	0.0033	0.0045	0.0022
λ_8	0.0421	0.0033	0.0031	0.0033	0.0045	0.0022
λ_9	0.0040	0.0059	0.0085	0.000	0.0069	0.0059
λ_{10}	0.000	0.000	0.000	0.000	0.000	0.000
λ_{11}	0.000	0.0017	0.000	0.000	0.000	0.000
λ_{12}	0.000	0.000	0.000	0.000	0.000	0.000

characteristics (like damping and frequency of oscillatory modes) over a wide range of variation for J_1 and J_2 in pu is presented in Figs. 10 and 11.

Fig. 10 presents the proper range of parameters for having the maximum index of damping factor. Fig. 11 also shows where the oscillatory index of the system could be minimum for different values of two control gains. For example, from Fig. 10, it can be observed that the minimum values for oscillatory index of studied system could achieved in the surface that the values of J_1 is higher than 1 and the values of J_2 is less than 0.5.

As a summary, these results show that a relatively acceptable performance can be obtained under small values of J_2 while system performance will reduce sharply for bigger value of this parameter. Appropriate results could be obtained when $J_1 > 0.6$ and $J_2 < 0.1$.

5 Simulation results

A thorough contingency analysis for different scenarios is necessary to evaluate the effects of proposed high level control and derivative-based virtual inertia's contribution for frequency control problem of interconnected systems. The test system is shown in Fig. 8 and the data are given by Rakhshani and Rodriguez [14]. In this study, three different scenarios are considered for further evaluation of system performance. The first scenario is based on severe step load disturbances as an input to the system. In the second scenario, the performance of the systems is evaluated after failing of one generation units in area 1. The last scenario is based on performance evaluation under trajectory sensitivity to plant parameter variation.

Table 5 Summary of eigenvalue sensitivity analysis

Element of state matrix ***A***	Sensitive modes	Participant states
$\alpha_{11,11}$	λ_1	ΔP_{ess1}
$\alpha_{12,12}$	λ_2	ΔP_{ess2}

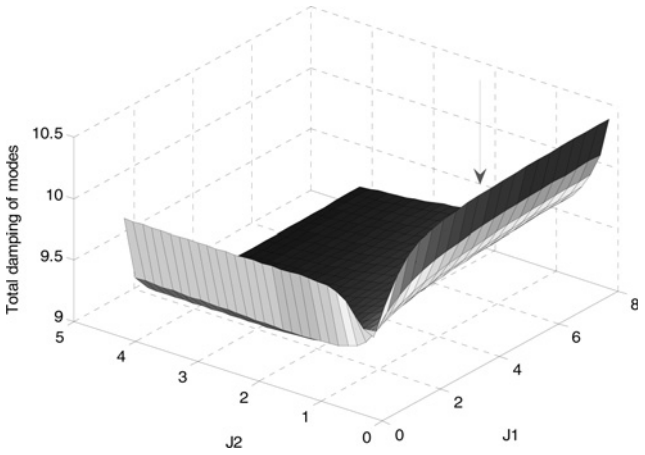

Fig. 10 *3D presentation for change in both control gains (J_1 and J_2) for total damping of oscillatory modes*

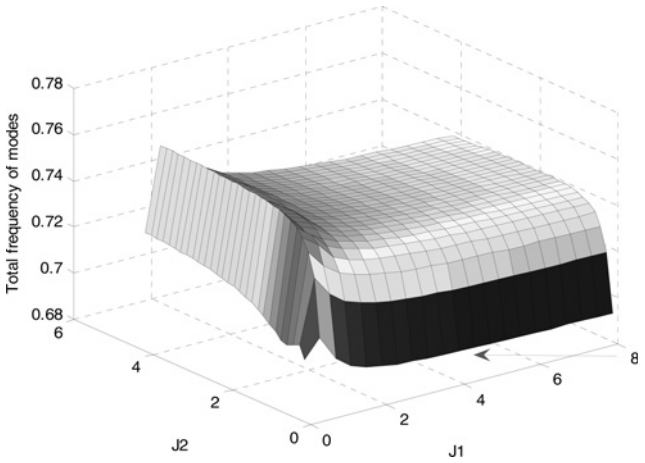

Fig. 11 *3D presentation for change in control gains (J_1 and J_2) for sum of the frequencies of oscillatory modes*

5.1 Scenario 1: General case study

In this scenario, it is assumed that two sequential step changes are happened. The first contingency is 0.03 pu load step change at 3 s in area 1 and the second is happening at 30 s by decreasing the demand to 0.015 pu. The control parameters of the studied power system are given in Table 6.

Frequency deviations in the first area and active power generation of unit 1 are presented in Figs. 12*a* and *b*, respectively. It is clear that by means of inertia emulation we are able to change the dynamic response of system and also the final response will be smoother than systems without storage capabilities.

The black dot-dash line is related to the system with HVDC link which shows for DC link will contribute only in damping of oscillation by improving the settling time of the system without especial improvements in first overshoot. However, after implementing the virtual inertia into the DC links, more improvements is appeared in reducing the first overshoots.

Table 6 Control parameters for studied model

Parameters	Value
K_{f1}	0.3
K_{f2}	0.1
K_{AC}	2.2
J_1	0.85
J_2	0.093

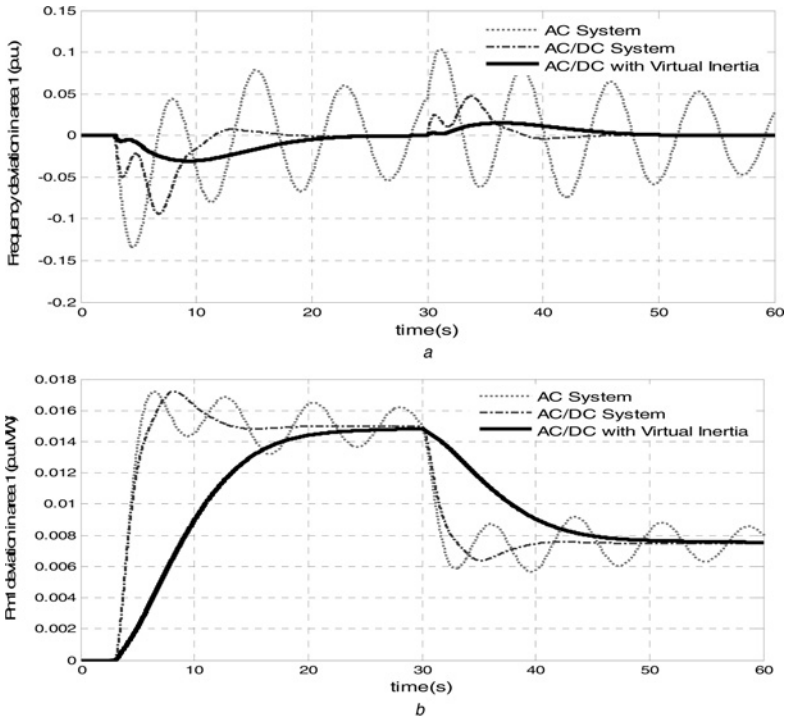

Fig. 12 *Dynamic responses of studied system*

a Frequency of area 1
b Generated power of unit 1

The DC and AC tie-line power flows are also presented in Figs. 13*a* and *b*, respectively. From the presented results, it can be observed that the fast controllable HVDC links helped to transfer sufficient emergency power to the disturbed area 1 with a satisfactory dynamic performance. The dynamic behaviours of the emulated power from both storage devices are also depicted in Fig. 14. Compared to the active power response in Fig. 12*b*, it is clear that the mechanical parts are very slow, while for the electronic ESS it can be observed that after a couple of seconds, at $t = 3.5$ s, the maximum emulated power can be reached.

Therefore, as shown in Fig. 14, the maximum discharging power which is emulating to the grid is 0.0262 at 3.5 s. In the second load

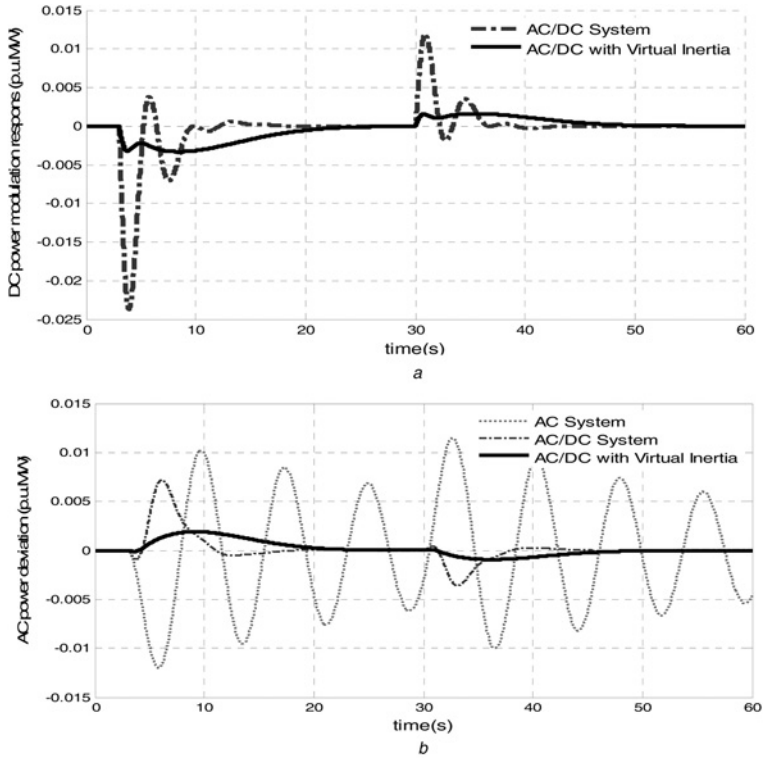

Fig. 13 *Dynamic responses of studied system*

a DC power
b AC power flow

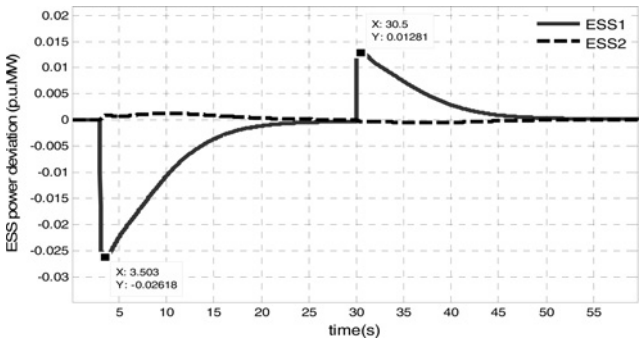

Fig. 14 *Status of emulated powers using derivative control*

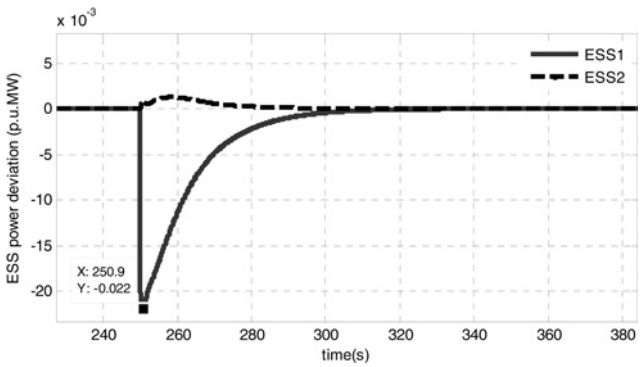

Fig. 16 *Status of emulated powers using derivative control*

change, we have a sudden decrease of demanded load in the same area 1. Due to this contingency, the frequency will increase. Therefore, the derivative control which is located in the same area (area 1), will start to be charged. Based on the obtained result, the maximum peak of variation is related to the ESS which is close to area 1 (the area with step load) which is also less 3% of the rated power. These values could identify the rating of necessity facilities for converter stations in DC link.

5.2 Scenario 2: Fail of generation unit

In the second contingency, we suppose one extreme situations. In this situation, after 250 s when the normal steady-state response is reached, the power generating unit1 in area 1 fails to operate. In these situations, the controller parameters are remaining unchanged. Frequency deviations in the first area and active power generation of unit 2 are presented in Figs. 15*a* and *b*, respectively.

Based on this simulation result, after cutting off the generating unit 1, the normal AC system is experiencing a significant change which will bring obvious oscillations. While the system with derivative-based inertia emulation is still able to effectively control the system output with little overshoot and negligible oscillations. It is obvious that after a while, other generation units will try to recover the loss of unit 1. This issue is shown in Fig. 15*b*, while the output of unit 2 in the same area is increasing. However, during the first overshoot and initial transient, a fast response ESS is helping the system by emulating inertia. As shown in Fig. 16, this emulated power mainly come from ESS1 in the same area of contingency.

5.3 Scenario 3: System parameter perturbation

In the last scenario, to examine the effectiveness of the proposed method on reduction of trajectory sensitivity to plant parameter variations, another case is simulated. In this case, previous

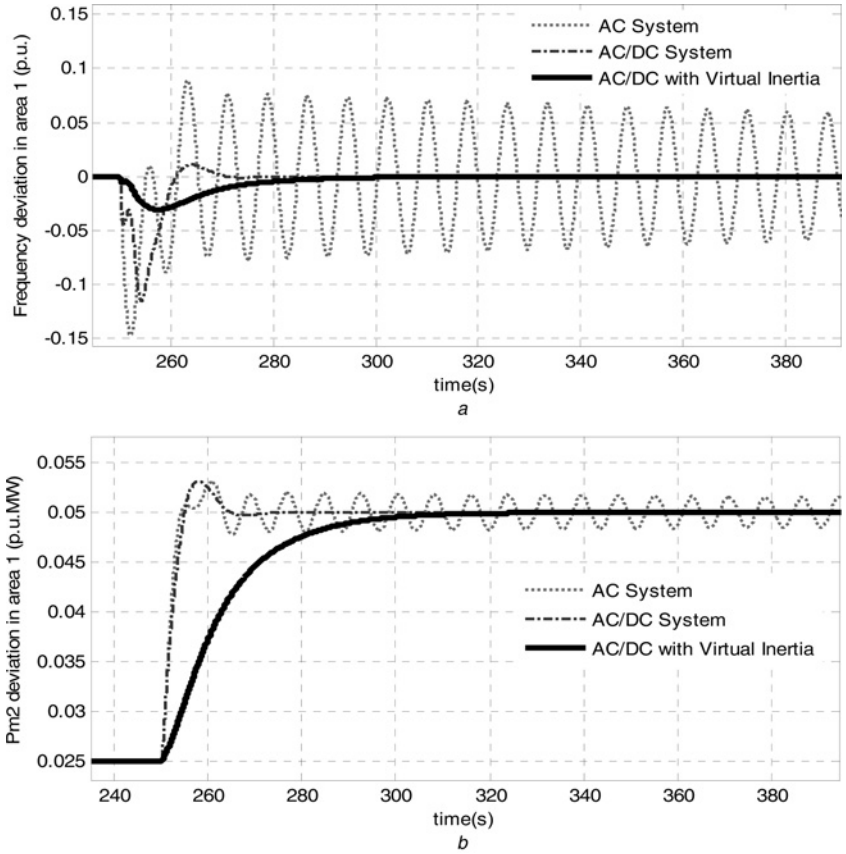

Fig. 15 *Dynamic responses for failing of unit 1 at 250 s*

a Frequency of area 1
b Generated power of unit 2

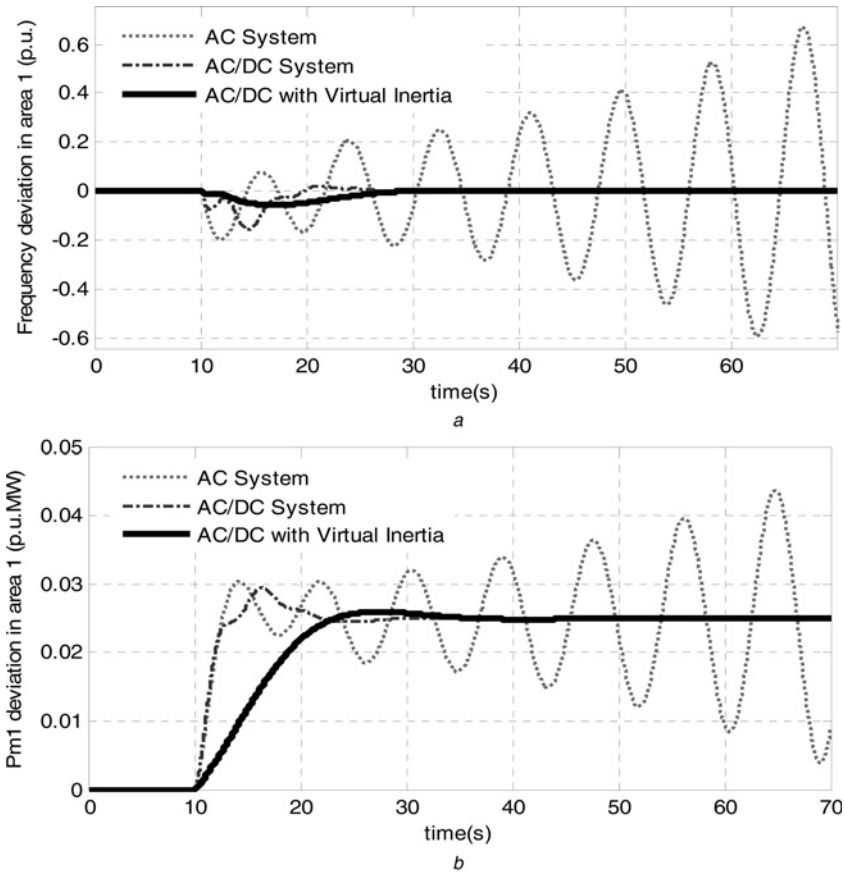

Fig. 17 *Dynamic responses of the system in third scenario*

a Frequency of area 1
b Generated power of unit 1

scenario in part 5.1, is simulated again with 25% increase in system parameters, i.e. generation unit's parameters and with 25% increase in demanded load by area 1.

The frequency deviation in area 1 and output of unit 1, with 25% increase in system parameters, are presented in Fig. 17*a* and *b*.

It is clear that the situation of normal AC system is totally critical and unstable while by using the proposed method, the oscillations are damped out in less than 20 s.

The dynamic response of DC tie-line power flows are also presented in Fig. 18. From presented results, it could be observed that the oscillation of tie-line power for AC/DC system is more than the one with inertia emulation capability. In practice, if the external reserve or storage capacities are large enough and the necessary amount of active power is less than the capacity of the HVDC interface, the frequency of each area could be restored to its nominal value quickly.

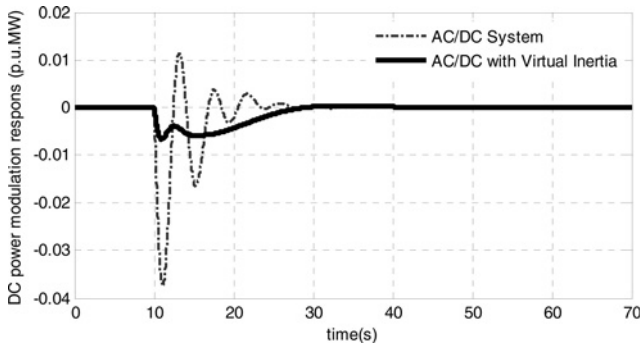

Fig. 18 *Dynamic responses of DC power flow in third scenario*

More details and comparisons about eigenvalues are also presented in Tables 7 and 8. Table 7 shows the eigenvalues of the power system for the third scenario.

From this table, it can be realised that two of the eigenvalues in normal AC system are on the right-hand side of the s-plane, which makes the normal AC system unstable. Another important point it that, the eigenvalues of proposed method are shifted to the

Table 7 Eigenvalues comparison for different systems

AC system	AC/DC system	AC/DC system with virtual inertia
0.0287 + 0.7343i	−24.2048	−166.64
0.0287 − 0.7343i	−0.2699 + 1.4727i	−49.34
−0.2435 + 0.3595i	−0.2699 − 1.4727i	−23.27
−0.2435 − 0.3595i	−0.2413 + 0.3722i	−0.83 + 1.64i
−0.5981	−0.2413 − 0.3722i	−0.83 − 1.64i
−2.0825	−0.8118	−0.15 + 0.21i
−2.2587	−2.1678 + 0.1450i	−0.15 − 0.21i
−2.6945	−2.1678 − 0.1450i	−0.24
−2.6316	−2.6889	−2.24
–	−2.6316	−2.53
–	–	−2.70
–	–	−2.63

Table 8 Comparisons of total damping factors of oscillatory modes for different systems

Index	AC system	AC/DC system	AC/DC system with virtual inertia
sum of damping factors	6.0437	7.4442	10.0561

left-hand side of the s-plane. Therefore, a better stability with less oscillatory modes (just four oscillatory modes) is observed. Furthermore, as shown in Table 8, the proposed method with less critical oscillatory modes has much higher damping factors.

6 Conclusions

Since the role of AGC is very important in the future modern power systems, proper adaptions and modifications will be predictable to take into accounts the new scenarios like market, high penetration of renewable generation and inertia emulations by power converter facilities.

In this paper, a general approach for implementing the virtual inertia in two-area AC/DC AGC interconnected system is proposed. Derivative control technique is used for control the stored energy of converter devices in AC/DC interconnected AGC power system. The proposed formulation could be easily implemented for any type of interconnected power systems with different size and characteristics. A complete sensitivity analysis for different control parameters was presented to show the real effects of inertia emulation for the system performance. Also more time domain simulation results for different contingency scenarios are presented. Analysis reveals that the proposed technique gives good results and usages of this method will reduce the peak deviations of frequencies and tie-line power with significant improvement of the system stability.

7 Acknowledgments

This work was partially supported by Spanish Science Ministry of Economy and competitiveness under the project ENE2013-48428-C2-2-R. Any opinions, findings and conclusions or recommendations expressed in this material are those of the authors and do not necessarily reflect those of the host institutions or funders.

8 References

1 Kunder, P.: 'Power system stability and control' (USA-McGraw-Hill, 1994)
2 Saadat, H.: 'Power system analysis' (McGraw-Hill, 1999)
3 Al-Haiki, Z.E., Shaikh-Nasser, A.N.: 'Power transmission to distant offshore facilities', *IEEE Trans. Ind. Appl.*, 2001, **47**, (3), pp. 1180–1183
4 Giddani, O.A., Abbas, A.Y.M., Adam, G.P., *et al*.: 'Multi-task control for VSC–HVDC power and frequency control', *Electr. Power Energy Syst.*, 2013, **53**, pp. 684–690
5 Fan, L., Miao, Z., Osborn, D.: 'Wind farms with HVDC delivery in load frequency control', *IEEE Trans. Power Syst.*, 2009, **24**, (4), pp. 1894–1895
6 Preece, R., Milanovic, J.V., Almutairi, A.M., *et al*.: 'Damping of inter-area oscillations in mixed AC/DC networks using WAMS based supplementary controller', *IEEE Trans. Power Syst.*, 2014, **28**, (2), pp. 1160–1169
7 Cuiqing, D., Agneholm, E., Olsson, G.: 'Use of VSC-HVDC for industrial systems having onsite generation with frequency control', *IEEE Trans. Power Deliv.*, 2008, **23**, (4), pp. 2233–2240
8 Du, Z.B., Zhang, Y., Liu, L., *et al*.: 'Structure-preserved power-frequency slow dynamics simulation of interconnected ac/dc power systems with AGC consideration', *IET Gener. Transm. Distrib.*, 2007, **1**, pp. 920–927
9 Jaleeli, N., VanSlyck, L.S., Ewart, D.N., Fink, L.H., Hoffmann, A.G.: 'Understanding automatic generation control', *IEEE Trans. Power Syst.*, 1992, **7**, (3), pp. 1106–1112
10 Rakhshani, E., Sadeh, J.: 'Practical viewpoints on load frequency control problem in a deregulated power system', *Energy Convers. Manage.*, 2010, **51**, (6), pp. 1148–1156
11 Ibraheem, A., Nizamuddin, A., Bhatti, T.S.: 'AGC of two area power system interconnected by AC/DC links with diverse sources in each area', *Electr. Power Energy Syst.*, 2014, **55**, pp. 297–304
12 Du, Z.B., *et al*.: 'Structure-preserved power-frequency slow dynamics simulation of interconnected ac/dc power systems with AGC consideration', *IET Gener. Transm. Distrib.*, 2007, **1**, (6), pp. 920–927
13 Bevrani, H., Hiyama, T.: 'Intelligent automatic generation control' (CRC Press, 2014, 2nd edn.)
14 Rakhshani, E., Rodriguez, P.: 'Active power and frequency control considering large scale RES', in Hossain, J., Mahmud, A. (Eds.), 'Large scale renewable power generation' (Springer-Verlag, 2013), pp. 233–271
15 Castillo, A., Gayme, D.F.: 'Grid-scale energy storage applications in renewable energy integration: A survey', *Energy Convers. Manage.*, 2014, **87**, pp. 885–894
16 Delille, G., François, B., Malarange, G.: 'Dynamic frequency control support by energy storage to reduce the impact of wind and solar generation on isolated power system's inertia', *IEEE Trans. Sustain. Energy*, 2012, **3**, (4), pp. 931–939
17 Aditya, S.K., Das, D.: 'Battery energy storage for load frequency control of an interconnected power system', *Electr. Power Syst. Res.*, 2001, **58**, pp. 179–185
18 Mufti, M.U.D., Shameem, A.L., Iqbal, S.J., *et al*.: 'Super-capacitor based energy storage system for improved load frequency control', *Electr. Power Syst. Res.*, 2009, **79**, (1), pp. 226–233
19 Sudha, K.R., Santhi, R.V.: 'Load frequency control of an interconnected reheat thermal system using type-2 fuzzy system including SMES units', *Electr. Power Energy Syst.*, 2012, **43**, pp. 1383–1392
20 Nomura, S., Tsutsui, S., Tsuji-Iio, S., *et al*.: 'Flexible power interconnection with SMES', *IEEE Trans. Appl. Supercond.*, 2006, **16**, (2), pp. 616–619
21 Abu-Siada Islam, S.: 'Application of SMES Unit in improving the performance of an AC/DC power system', *IEEE Trans. Sustain. Energy*, 2011, **2**, (2), pp. 109–121
22 Zhu, J., Booth, C.D., Adam, G.P., *et al*.: 'Inertia emulation control strategy for VSC-HVDC transmission system', *IEEE Trans. Power Syst.*, 2013, **28**, (2), pp. 1277–1287
23 Zhang, L., Harnefors, L., Nee, H.P.: 'Power-synchronization control of grid-connected voltage-source converters', *IEEE Trans. Power Syst.*, 2010, **25**, pp. 809–820
24 Zhong, Q.C., Nguyen, P.L., Ma, Z., *et al*.: 'Self-synchronized synchronverters: inverters without a dedicated synchronization unit', *IEEE Trans. Power Electron.*, 2014, **29**, (2), pp. 617–630
25 Rodriguez, P., Candela, I., Citro, C., *et al*.: 'Control of grid-connected power converters based on a virtual admittance control loop'. Proc. European Conf. on Power Electronics and Applications (EPE), 2013
26 Lee, D.J., Wang, L.: 'Small-signal stability analysis of an autonomous hybrid renewable energy power generation/energy storage system part I: time-domain simulations', *IEEE Trans. Energy Convers.*, 2008, **23**, (1), pp. 311–320
27 Datta, M., Ishikawa, H., Naitoh, H., *et al*.: 'LFC by coordinated virtual inertia mimicking and PEVs in power utility with MW-class distributed PV generation'. IEEE 13th Workshop on Control and Modeling for Power Electronics (COMPEL), 2011, pp. 1–8
28 Ray, P.K., Mohanty, S.R., Kishor, N.: 'Proportional–integral controller based small-signal analysis of hybrid distributed generation systems', *Energy Convers. Manage.*, 2011, **52**, pp. 1943–1954
29 Yan, R., Saha, T.K.: 'Frequency response estimation method for high wind penetration considering wind turbine frequency support functions', *IET Renew. Power Gener.*, 2015, **9**, (7), pp. 775–782
30 Van de Vyver, J., De Kooning, J.D.M., Meersman, B., *et al*.: 'Droop control as an alternative inertial response strategy for the synthetic inertia on wind turbines', *IEEE Trans. Power Syst.*, 2015, **PP**, (99), pp. 1–10
31 Gonzalez-Longatt, F.M.: 'Effects of the synthetic inertia from wind power on the total system inertia: simulation study'. Int. Symp. on Environment Friendly Energies and Applications (EFEA), 2012, pp. 389–395
32 Driesen, J., Visscher, K.: 'Virtual synchronous generators'. IEEE Proc. on Power and Energy Society – General Meeting, 2008, pp. 1–3
33 Donde, V., Pai, A., Hiskens, I.A.: 'Simulation and optimization in an AGC system after deregulation', *IEEE Trans. Power Syst.*, 2001, **16**, (3), pp. 481–489
34 Datta, M., Senjyu, T., Yona, A., *et al*.: 'A frequency-control approach by photovoltaic generator in a PV – diesel hybrid power system', *IEEE Trans. Energy Convers.*, 2011, **26**, pp. 559–571
35 Pourmousavi, S.A., Nehrir, M.H.: 'Introducing dynamic demand response in the LFC model', *IEEE Trans. Power Syst.*, 2014, **29**, (4), pp. 1562–1572
36 Chidambaram, I.A., Paramasivam, B.: 'Control performance standards based load-frequency controller considering redox flow batteries coordinate with interline power flow controller', *J. Power Sources*, 2012, **219**, pp. 292–304